Enhancing Plasmonic Spectral Tunability with Anomalous Material Dispersions

Mengjie Zheng[1,2,3], Yi Yang[3,*], Di Zhu[3,4], Yiqin Chen[1], Karl K. Berggren[3], Marin Soljačić[3] and Huigao Duan[1,*]

[1] College of Mechanical and Vehicle Engineering, State Key Laboratory of Advanced Design and Manufacturing for Vehicle Body, Hunan University, 410082 Changsha, China

[2] Jihua Laboratory, 528000 Foshan, China

[3] Research Laboratory of Electronics, Massachusetts Institute of Technology, 02139 Cambridge, MA, USA

[4] John A. Paulson School of Engineering and Applied Sciences, Harvard University, 02138 Cambridge, MA, USA

[*]Addresses correspondence to yiy@mit.edu (Y.Y.) and duanhg@hnu.edu.cn (H.D.)

Abstract

Plasmonic nanoresonators confine and enhance strong electromagnetic fields beyond the diffraction limit. Under structural variations or environmental perturbations, such strong confinement enables superior spectral tunability, which serves as the basic operating principle for nanorulers, sensors, color displays, and broadband optoelectronic devices. To date, properties of material dispersion have seldom been exploited in order to achieve a wide spectral tunability. In this work, we propose and demonstrate that materials with anomalous dispersion, such as germanium (Ge) in the visible, enable improved spectral tunability for plasmonic nanoresonators. We theoretically introduce our proposal with a semi-analytical guided mode picture, where the spectral tunability of open resonators can be evaluated by sampling the plasmon dispersion of the associated closed systems at resonant wavevectors. Experimentally, using Ge-based film-coupled gap plasmon resonators as an example, we fabricate two experimental architectures and demonstrate the improved spectral tunability with single-particle dark-field scattering spectroscopy and plasmonic color generation. In single Ge-Au structures, we achieve an absolute and relative shift of ~ 100 nm and

~ 17%, respectively, in the visible wavelength regime, for a ~10-nm gap size variation. Such measured tunability achieves a more than 3-fold improvement than that of materials with normal dispersion (such as Si in the visible). In large array systems made of inversely fabricated Ge-Ag resonators, we demonstrate the tunability of plasmonic color generation and wide color gamut under various gap sizes. Our results introduce anomalous material dispersion as an extra useful degree of freedom to engineer the spectral tunability of plasmonic systems, especially relevant for actively tunable plasmonics and metasurfaces.

Keywords: plasmonic resonances, spectral tunability, anomalous dispersion, color display

Plasmonic nanostructures allow us to manipulate electromagnetic waves at the subwavelength regime[1, 2]. A few quintessential plasmonic nanoresonators include dimers[3-5], trimers[6, 7], bowtie nanoantennas[8, 9], and film-coupled nanoparticles[10, 11]. These structures play a prominent role in both fundamental studies and relevant applications[12]. Recently, beyond static architectures, tunable plasmonics[13, 14] has evolved into a research focus and it can potentially enable a variety of applications such as active metasurfaces[15, 16], plasmonic color generation[17-19], tunneling transistors[20-22], plasmonic nanorulers[23, 24], and accurate sensors[25, 26]. Among various strategies, the incorporation of micro/nano-electromechanical systems with plasmonic nanostructures[27] is a promising direction. In this case, the spectral tunability under structural variations becomes a prominent figure-of-merit to optimize. For this purpose, the film-coupled gap-plasmon nanoresonators[11, 28, 29], whose resonances are known to be sensitive to their gap sizes, are natural candidates to consider.

The film-coupled gap-plasmon nanoresonators can be fabricated with relative ease, by either top-down lithography or bottom-up chemistry synthesis. The upper nanoantennas can be metals or high-index dielectrics, depending on the wavelength and radiative efficiency of interest. In such gap-plasmon structures, the fundamental dipolar

resonances, which couple to free-space plane-wave excitations, exhibit superior spectral tunability in tandem with strong scattering and absorption. For metal-insulator-metal (MIM) configurations, if patch nanoantennas (such as disks and cubes) are employed, the spectral tunability by varying gap sizes is limited to the infrared regime[30] for nanoantennas of tens of nanometer sizes and gap sizes of few nanometers. Alternatively, for tapered-shape antennas[31] (such as spheres and ellipses) where the gap plasmons are no longer confined underneath the entire antenna footprint, the resonance can be shifted to the visible regime at the cost of reduced spectral tunability[32]. Furthermore, nonclassical corrections of different origins can become non-negligible because of the extremely nanoscopic gap sizes[32-35]. For noble metals such as Ag and Au, which are the most commonly used plasmonic materials, these corrections further blueshift the resonance, resulting in a reduced spectral tunability. On the other hand, there have been complementary studies of the hybrid dielectric gap-plasmon nanoresonators[36, 37], where high-index dielectric nanoparticles couple to metallic substrates. This simple reconfiguration enables strong, tunable plasmonic response in the visible regime and is recently found to exhibit robustness against the detrimental nonclassical corrections[33]. So far, the spectral tunability of the gap plasmon resonances mostly relies on their waveguide/geometric dispersion. In contrast, material dispersions, which can be of engineering utility as we will show below, are typically neglected compared to the strong slow-light effect of the gap plasmons.

In this work, we propose that anomalous material dispersion (i.e. increased permittivity/refractive index towards longer wavelengths), such as germanium (Ge) in the visible regime[38, 39], can be utilized to achieve a wide plasmon tunability. Theoretically, we explain the intuition with a simple guided mode picture for the gap-plasmon resonances. Experimentally, we first study in detail the spectral tunability of Ge-Au gap plasmons by measuring single-particle scattering of Ge nanodisks on Au-coated substrates with controlled nanometer dielectric gaps. We then extend the concept to plasmonic color generation and demonstrate its tunability as a function of gap sizes in an inversely fabricated Ge nanodisk array on a silver reflector, an architecture that delivers vibrant color and prevents material oxidation. Our work reveals the utility of

anomalous material dispersion for improving the spectral tunability of plasmonic resonances, which provides a useful design principle for tunable plasmon devices. Specifically, actively tunable plasmons can be generated by replacing the static spacer with tunable materials, such as electrically-tunable molecular thin film[22], or including movable nanostructured components[27, 34]. This approach could enable future active plasmonic devices and metasurfaces, such as paper/canvas-like full-color displays and nanoscale sensors with wide dynamic ranges.

We start by providing a simple theoretical understanding for the utility of anomalous material dispersion in the spectral tunability of plasmons. The material dispersions of two common high-index materials, bulk undoped Ge and Si, in the visible wavelengths are shown in Fig. 1a and b. Si exhibits normal dispersion throughout, while Ge exhibits anomalous dispersion from 430 to 600 nm. Both Ge and Si nanostructures, as alternatives of their all-metallic counterparts, have been utilized to achieve gap plasmon resonances[37, 40]. Intuitively, these gap-plasmon resonances in open systems can be understood as the surface plasmons of a closed planar multilayer system restricted to specific quantized resonant wavevectors[36].

Therefore, in Fig. 1c-e, we calculate the dispersion curves of the highly-confined gap plasmon in three different dielectric-dielectric-metal (DDM) waveguide systems, where the upper dielectric layers are dispersionless material (refractive index n = 4.5), Ge, and Si, respectively. We compute the dispersion at different gap sizes (g = 1 nm, 2 nm, and 4 nm) for each multilayer systems. The sampling of the dispersions, at a given resonant momentum k_{res}, indicates the plasmon spectral tunability of the associated open system[36]. For example, at $k_{\mathrm{res}} \approx 1.6k_{\mathrm{p}}$ (black solid line; k_{p} is the wave vector of light in free space at the plasma frequency), the fictitious dispersionless material, Ge, and Si achieve spectral tunability (shaded yellow) of ~140 nm, ~180 nm, and ~100 nm, respectively. It is thus evident that anomalous (normal) material dispersion increases (decreases) the spectral tunability of gap plasmons. This conclusion is consistent with intuition--a smaller gap confines plasmons more tightly in the dielectric gap and causes redshifts, or equivalently, increases the effective indices and shifts the plasmons

towards longer wavelengths, which is the same (revised) direction of the anomalous (normal) material dispersion.

We numerically verify the relation between material dispersion and spectral tunability, predicted from the above analysis of the closed waveguide systems, in open resonators. Specifically, we truncate the uniform upper dielectric layers into nanodisks. The DDM waveguides thus become film-coupled nanoresonators. In Fig. 1f and g, we calculate the reflection spectra, at normal incidence, of Ag thin film-coupled Ge and Si nanodisk arrays, respectively. The structural parameters are chosen such that the resonance dips fall within the anomalous dispersion wavelengths of Ge. As the gap size varies from 8 nm to 1 nm, the Ge gap-plasmon nanoresonator shows a spectral red-shift of ~230 nm while that of the Si nanoresonator is ~150 nm. The contrasting spectral tunability in the two cases (Fig. 1f and g) is consistent to that in their closed system counterparts (Fig. 1d and e). Taken together, our analysis, in both closed and open systems, reveals the utility of anomalous material dispersion in enhancing the spectral tunability of plasmonic resonances.

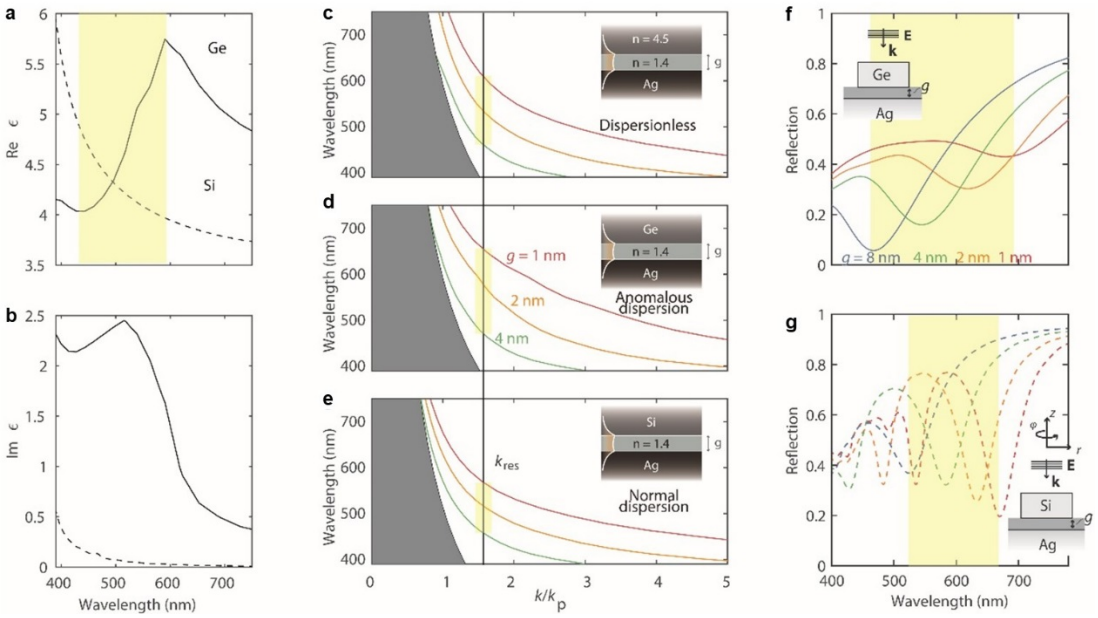

Figure 1 Anomalous plasmon dispersion for wide plasmon tunability. **a-b.** Material dispersion of two high-index dielectric materials, Si and Ge (material index taken from Palik[41]) in the visible wavelengths. Ge exhibits strong anomalous dispersion (shaded yellow in a) while Si shows normal dispersion. **c-e.** Gap plasmon dispersion relations for closed systems, specifically, dielectric-dielectric (n = 1.4)-metal (Ag, optical

constant taken from Johnson and Christy[42]) waveguides, where the upper dielectric layers are made from a dispersionless material (n = 4.5), Ge and Si from **c** to **e** respectively (see insets). The plasmon spectral tunability, due to gap size variations, can be obtained by sampling the dispersions at a fixed resonant momentum k_{res}. Ge (Si), showing anomalous (normal) dispersion, exhibit the widest (narrowest) spectral tunability. We choose the plasma frequency of Ag as 9 eV. The shaded grey regions are light cones. **f-g.** Spectral tunability (shaded yellow) of gap plasmon resonances in open resonators, specifically, film-coupled Ge (**f**) and Si (**g**) nanodisks. For the same gap size variation (1-8 nm), the spectral tunability of Ge is 1.8 times wider than that of Si. Here the gap has a refractive index of 1.4, the disk height is 60 nm, and the disk diameters are 75 nm and 105 nm for Ge and Si, respectively. The array periodicities are twice the particle diameters.

To demonstrate the spectral tunability in the presence of anomalous material dispersion, we measured the single-particle scattering of Ge gap-plasmon nanoresonators using dark-field spectroscopy. Figure 2a shows the experimental structure ---Ge nanodisk arrays atop an Au substrate, separated by an AlO_x layer grown using atomic layer deposition (ALD). The fabrication details can be found in Fig. S1. Au was chosen as the reflector substrate material instead of Ag (as shown in Fig. 1f and g) to avoid natural oxidization. Adjacent nanodisks were well-separated (pitch: 5 μm) to ensure the validity of single-particle treatment in our simulation. As shown in Fig. 2b, we measured the permittivity of the thermally evaporated Ge thin film using an ellipsometer. Different from the bulk permittivity[43] (tangerine solid line), the anomalous dispersion of the evaporated Ge (46 nm) spans the entire visible light regime, which facilitates the verification of our predictions in a wider wavelength window. The optical constant of 2-nm-thick Ge ultrathin film from Ciesielski[44] was also plotted for reference, confirming that the dispersion of Ge film depends on its thickness. A dark-field optical micrograph of a fabricated Ge nanoresonator array (disk diameter 80 nm and gap size 8.3 nm) was shown in Fig. 2c, showing uniform scattering intensity across individual nanodisks.

We probed the fundamental dipolar gap plasmon resonances (simulated field profiles shown in Supplementary Fig. S2) with single-particle dark-field scattering spectroscopy. Specifically, scattered signals were recorded for single Ge nanoresonators spanning three diameters (D = 90 nm, 80 nm and 70 nm) and five gap sizes, i.e. AlO_x layer thicknesses ($t \approx$ 11.4 nm, 8.3 nm, 4.9 nm, 2.9 nm and 0 nm). The gap sizes were ellipometrically determined, in accordance with the nominal ALD cycles (see in Supplementary Fig. S3). As shown in Fig. 2d, with decreasing gap size, monotonic ~100 nm redshifts of the resonances for all disk diameters were observed. We note that the measured redshift is about half of the theoretical prediction. The major reason is that the anomalous dispersion is less strong in evaporated Ge than that in bulk Ge in the visible regime (see Fig. 2b). The simulated spectra in Fig. 2e adopt the measured refractive index of Ge and agree well with the measurements in Fig. 2d. We note that when the gap size decreases, the scattering intensity drops because of the reduced radiative efficiency under stronger light confinement. In contrast, if the upper nanoresonators were replaced by Si nanodisks, under normal material dispersion, the spectral shifts reduce to < 30 nm for the similar range of gap size variation[33] (Fig. S4, Supplementary Information).

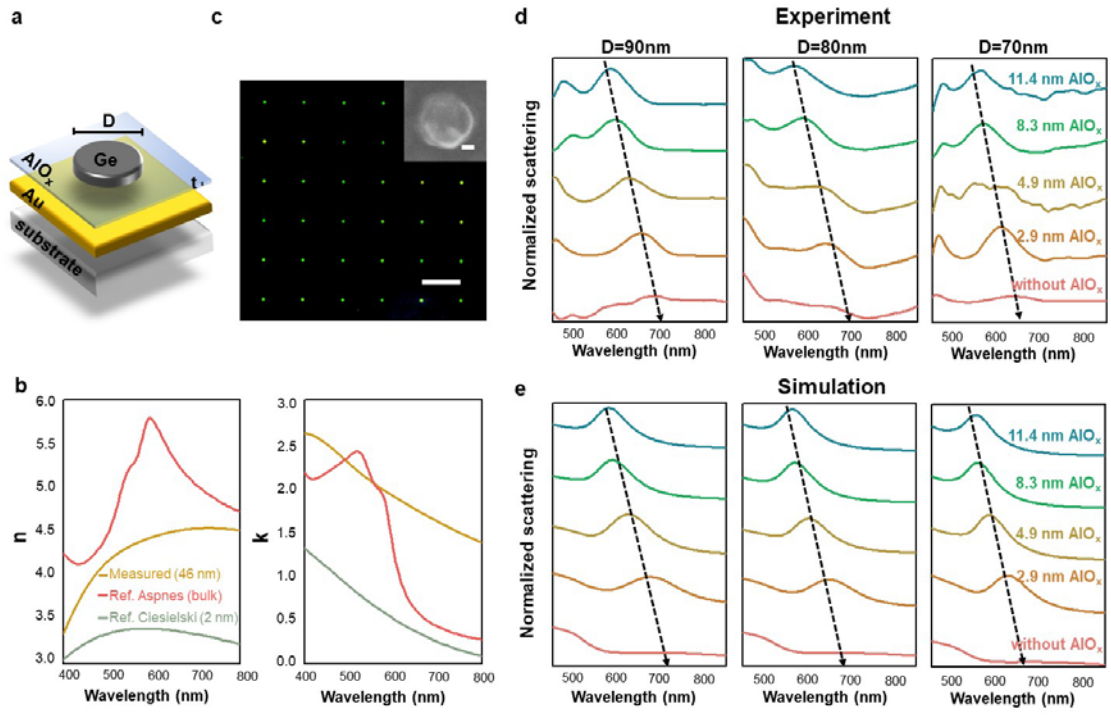

Figure 2 Measurement of plasmon tunability under anomalous material dispersion. **a.**

Schematic of a Ge-Au gap-plasmon nanoresonator. The substrate is coated with an ultrathin AlO_x layer and an Au back reflector. **b.** Measured permittivity of evaporated Ge material (46 nm), compared with bulk and a referenced ultrathin film. **c.** A typical dark-field optical micrograph of an 80-nm-diameter Ge nanodisk array with 8.3 nm gap size. Inset, scanning electron micrograph (SEM) image of an individual Ge nanodisk. **d-e.** Measured (**d**) and simulated (**e**) spectral tunability of Ge gap plasmon resonators. Scale bars: 5 μm for **b** and 20 nm for inset in **b**.

Next, as an engineering example of anomalous material dispersion, we demonstrate a Ge-based plasmonic color printing to further highlight the spectral tunability and fabrication scalability. Figure 3a shows the schematic of the cross-section of a unit cell. Here, we replaced the Au reflector with Ag and used an inverse fabrication process to prevent oxidations (see Fig. S5 in the Supplementary Information for details on the fabrication). In this design, structures were fabricated on a transparent substrate (quartz) and inspected from the backside. Compared to Au, Ag has a flatter reflection spectrum in the visible, and therefore provides a purer white background and creates more vibrant colors[45-47]. Furthermore, the inverse fabrication process encapsulates the Ge, which also prevents oxidation of Ag (at the Ag-AlO_x interface).

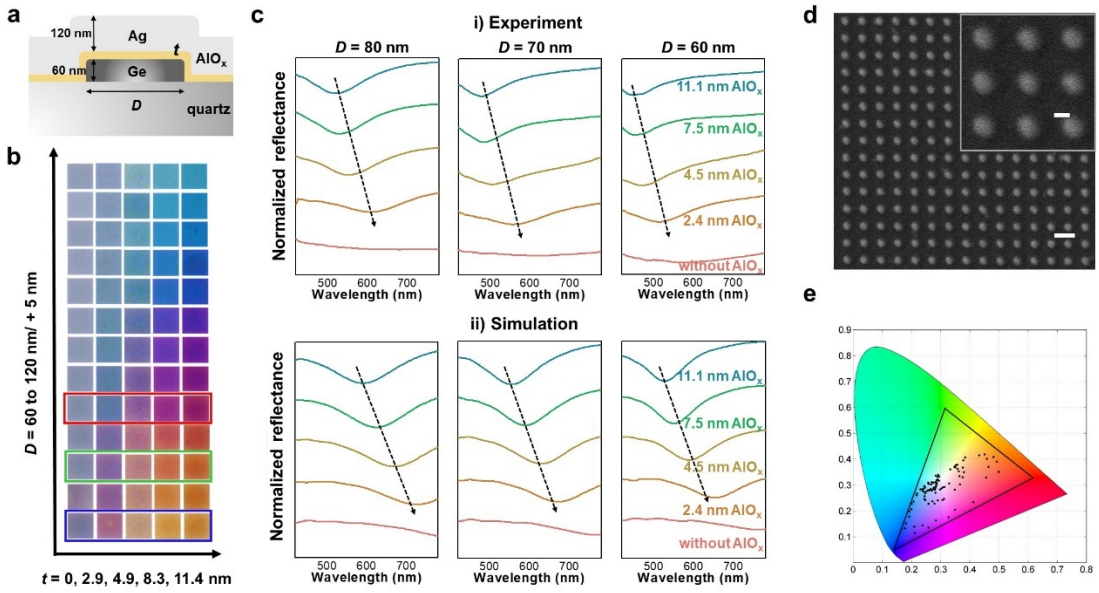

Figure 3 Anomalous-dispersion-based Ge gap-plasmon nanoresonators for color printing. **a.** Cross-sectional schematic of a unit cell of a film-coupled Ge nanoresonator

array, featured by ultrathin AlO_x and optically thick silver film inversely coating the quartz substrate. **b.** Color palette with diameter variations (D = 60 to 120 nm) of Ge nanodisks at a step size of 5 nm for varying AlO_x layer thickness ($t \approx 0$ nm, 2.4 nm, 4.5 nm, 7.5 nm, 11.1 nm). **c.** Experimental (i) and simulated (ii) reflection spectra of the color tiles labelled by red (D = 80 nm), green (D = 70 nm) and blue (D = 60 nm) solid frame in **b**. The black dashed arrows represent the dip shift trend. **d.** SEM images of Ge nanodisks with D = 80 nm before the ALD process. **e.** CIE 1931 chromaticity coordinates of the measured reflection spectra of the color palette in **a**. Scale bars: 200 nm for **c**, and 50 nm for inset in **c**.

We first created color palettes by patterning square arrays of Ge nanodisks with varying diameter (D) and gap sizes (t). Figure 3b shows the bright-field optical micrographs of the palette. The disk diameter D increases from 60 nm to 140 nm with 5 nm steps along the y axis, and the gap size ($t \approx 0$, 2.4 nm, 4.5 nm, 7.5 nm, and 11.1 nm) increases along the x axis. For each array, the spacing between adjacent nanodisks was set to be the same as the diameter to ensure a consistent fill factor. The reflection colors change under various nanodisk diameters and gap sizes. The fact that the colors can be tuned prominently by only a few nanometer change in the gap size is especially relevant for active color/spectral control[48] using nanoelectromechanical means[22], where the gap size can be controlled dynamically.

Figure 3c shows the measured and simulated reflection spectra of the color tiles labeled in Fig. 3b (D = 80 nm, 70 nm, and 60 nm respectively). For a fixed nanodisk diameter, e.g. D = 60 nm, the measured spectral shift is ~130 nm for gap sizes t between 0 and 11.1 nm. Taking Ge native oxidation after evaporation into consideration, a 3-nm-thick GeO_x film (optical constant taken from Nunley[49]) was added to coat the Ge nanoresonator in the computational model. Compared with numerical simulations, a blueshift of the resonant dip was observed in the measurements, which could result from the imperfections during fabrication process, such as the air-hole defects[50] at the edge of the nanodisks. Nevertheless, in terms of spectral tunability, the experimental spectra agree well with simulations. Figure 3d shows a typical SEM image of a Ge

nanodisk array (D = 80 nm, t = 7.5 nm) on quartz substrate before the ALD process. As shown in Fig. 3e, all the reflection data of the extended color palettes were transformed into the CIE 1931 chromaticity coordinates. The color palettes enclose a wide gamut. Therefore, the anomalous-dispersion-based scheme is compatible for the requirement of vivid color generation and could also be useful for full-color printing applications.

We also exploited the color variation from pitches (P) and disk diameter (D) (see Supplementary Fig. S6) to form an extended color database. The established database contains the correlated information about the geometries (D and P) and the RGB values obtained from the reflection spectra per data element. With this database, we were able to implement photorealistic color printing. Here, we fabricated two full-color microprints of a Chinese ink painting with two different dielectric spacer thicknesses (2.4 nm and 7. 5 nm). The target original digital image shown in Fig. 4a was pixelized and converted into a final fabrication layout by automatically matching closest RGB colors using a Python script. Each physical pixel was 1 μm × 1 μm, which includes multiple nanodisks with certain diameter and pitch. The two microprints were fabricated using the same inverse fabrication process depicted in Fig. 3a. Figure 4b and c show the bright-field optical micrographs of the fabricated paintings (250 μm × 150 μm) with AlO_x gap sizes of ~2.4 nm and ~7.5 nm, respectively. The two paintings show a significant difference in color despite of the nanoscale variation of the dielectric spacer thickness, consistent the predicted strong spectral tunability. Similar color tunability was reproduced in another piece of painting with a different color scheme (see Supplementary Fig. S7).

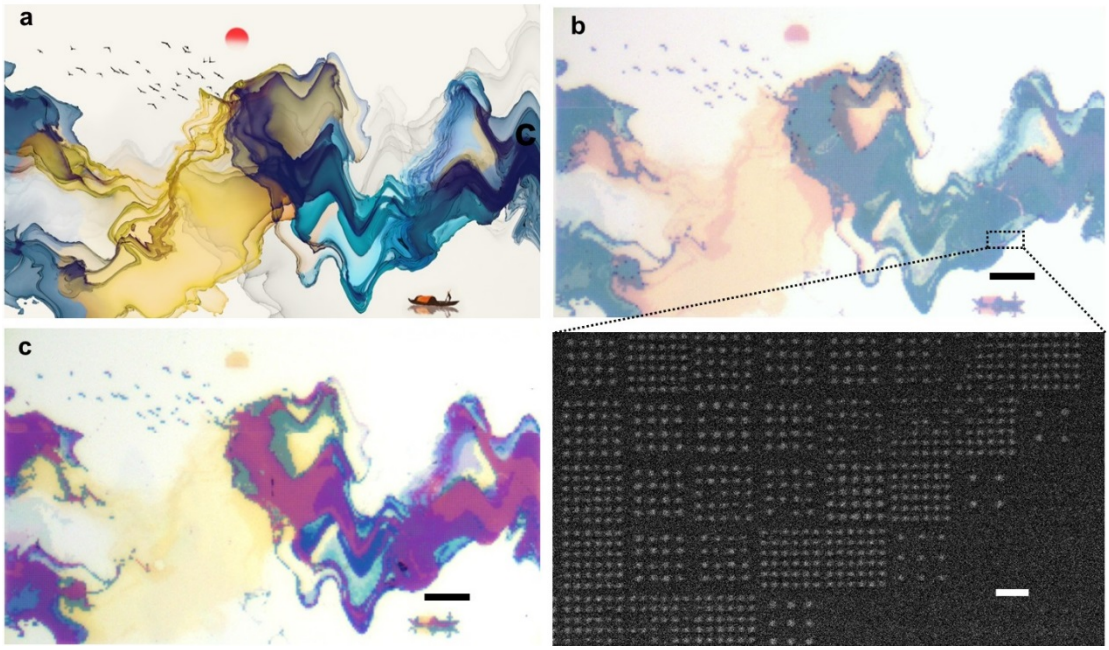

Figure 4 Reproducing vivid microprints using different AlO_x gap sizes. **a.** The original Chinese ink painting. **b-c.** Optical micrographs of Ge nanoresonators with 2.4 nm (**b**) and 7.5 nm (**c**) thick AlO_x dielectric layers. **d.** The corresponding SEM micrograph of the labelled area by the black solid frame. Scale bars: 20 μm for **b** and **c**; 500 nm for **d**.

In summary, we have proposed that anomalous material dispersion enables improved spectral tunability of plasmonic resonances. As an example, we illustrated our proposal with Ge in the visible wavelengths. Two Ge gap-plasmon resonators architectures were developed to demonstrate the wide plasmon tunability using single-particle scattering spectroscopy and reflection measurements. We expanded such a gap plasmon architecture for color generation. Under few-nanometer variation of the spacer thickness, the observed color change reveals the potential for tunable color printing. Future efforts include oxidization prevention, engineering the optical responses of Ge and other materials for stronger anomalous dispersion at various spectral windows, and integration of static nanostructures with actuators and controls for tunable plasmonic and metamaterial devices.

Acknowledgement

This work was supported in part by the ONR grant N00014-17-1-2977, as well as in

part by the U. S. Army Research Office through the Institute for Soldier Nanotechnologies at MIT, under Collaborative Agreement Number W911NF-18-2-0048, and in part by the MRSEC Program of the National Science Foundation under award number DMR - 1419807."

Reference

1. Brongersma, M. L.; Shalaev, V. M. *Science* 2010, 328, (5977), 440-441.
2. Novotny, L.; Van Hulst, N. *Nat. Photon.* 2011, 5, (2), 83.
3. Zuloaga, J.; Prodan, E.; Nordlander, P. *Nano Lett.* 2009, 9, (2), 887-891.
4. Marinica, D. C.; Kazansky, A. K.; Nordlander, P.; Aizpurua, J.; Borisov, A. G. *Nano Lett.* 2012, 12, (3), 1333-1339.
5. Scholl, J. A.; García-Etxarri, A.; Koh, A. L.; Dionne, J. A. *Nano Lett.* 2013, 13, (2), 564-569.
6. Fan, J. A.; Wu, C.; Bao, K.; Bao, J.; Bardhan, R.; Halas, N. J.; Manoharan, V. N.; Nordlander, P.; Shvets, G.; Capasso, F. *Science* 2010, 328, (5982), 1135-1138.
7. Sheikholeslami, S. N.; García-Etxarri, A.; Dionne, J. A. *Nano Lett.* 2011, 11, (9), 3927-3934.
8. Fromm, D. P.; Sundaramurthy, A.; Schuck, P. J.; Kino, G.; Moerner, W. *Nano Lett.* 2004, 4, (5), 957-961.
9. Duan, H.; Fernández-Domínguez, A. I.; Bosman, M.; Maier, S. A.; Yang, J. K. *Nano Lett.* 2012, 12, (3), 1683-1689.
10. Akselrod, G. M.; Argyropoulos, C.; Hoang, T. B.; Ciracì, C.; Fang, C.; Huang, J.; Smith, D. R.; Mikkelsen, M. H. *Nat. Photon.* 2014, 8, (11), 835.
11. Moreau, A.; Ciracì, C.; Mock, J. J.; Hill, R. T.; Wang, Q.; Wiley, B. J.; Chilkoti, A.; Smith, D. R. *Nature* 2012, 492, (7427), 86.
12. Giannini, V.; Fernández-Domínguez, A. I.; Heck, S. C.; Maier, S. A. *Chem. Rev.* 2011, 111, (6), 3888-3912.
13. Manjavacas, A.; De Abajo, F. G. *Nat. Commun.* 2014, 5, 3548.
14. Yao, Y.; Shankar, R.; Kats, M. A.; Song, Y.; Kong, J.; Loncar, M.; Capasso, F. *Nano Lett.* 2014, 14, (11), 6526-6532.
15. Sautter, J.; Staude, I.; Decker, M.; Rusak, E.; Neshev, D. N.; Brener, I.; Kivshar, Y. S. *ACS Nano* 2015, 9, (4), 4308-4315.
16. Holsteen, A. L.; Cihan, A. F.; Brongersma, M. L. *Science* 2019, 365, (6450), 257-260.
17. Yokogawa, S.; Burgos, S. P.; Atwater, H. A. *Nano Lett.* 2012, 12, (8), 4349-4354.
18. Duan, X.; Kamin, S.; Liu, N. *Nat. Commun.* 2017, 8, 14606.
19. Kumar, K.; Duan, H.; Hegde, R. S.; Koh, S. C.; Wei, J. N.; Yang, J. K. *Nat. Nanotechnol.* 2012, 7, (9), 557.
20. Ju, L.; Geng, B.; Horng, J.; Girit, C.; Martin, M.; Hao, Z.; Bechtel, H. A.; Liang, X.; Zettl, A.; Shen, Y. R. *Nat. Nanotechnol.* 2011, 6, (10), 630.
21. Fei, Z.; Iwinski, E.; Ni, G.; Zhang, L.; Bao, W.; Rodin, A.; Lee, Y.; Wagner, M.; Liu, M.; Dai, S. *Nano Lett.* 2015, 15, (8), 4973-4978.
22. Niroui, F.; Wang, A. I.; Sletten, E. M.; Song, Y.; Kong, J.; Yablonovitch, E.;

Swager, T. M.; Lang, J. H.; Bulovic, V. *ACS Nano* 2015, 9, (8), 7886-7894.
23. Butet, J.; Martin, O. J. *ACS Nano* 2014, 8, (5), 4931-4939.
24. Liu, N.; Hentschel, M.; Weiss, T.; Alivisatos, A. P.; Giessen, H. *Science* 2011, 332, (6036), 1407-1410.
25. Hao, F.; Nordlander, P.; Sonnefraud, Y.; Dorpe, P. V.; Maier, S. A. *ACS Nano* 2009, 3, (3), 643-652.
26. El-Zohary, S. E.; Azzazi, A. A.; Okamoto, H.; Okamoto, T.; Haraguchi, M.; Swillam, M. A. *J. Nanophoton.* 2013, 7, (1), 073077.
27. Holsteen, A. L.; Raza, S.; Fan, P.; Kik, P. G.; Brongersma, M. L. *Science* 2017, 358, (6369), 1407-1410.
28. Nielsen, M. G.; Gramotnev, D. K.; Pors, A.; Albrektsen, O.; Bozhevolnyi, S. I. *Opt. Express* 2011, 19, (20), 19310-19322.
29. Mock, J. J.; Hill, R. T.; Tsai, Y.-J.; Chilkoti, A.; Smith, D. R. *Nano Lett.* 2012, 12, (4), 1757-1764.
30. Akselrod, G. M.; Huang, J.; Hoang, T. B.; Bowen, P. T.; Su, L.; Smith, D. R.; Mikkelsen, M. H. *Adv. Mater.* 2015, 27, (48), 8028-8034.
31. Faggiani, R. m.; Yang, J.; Lalanne, P. *ACS Photonics* 2015, 2, (12), 1739-1744.
32. Ciracì, C.; Hill, R.; Mock, J.; Urzhumov, Y.; Fernández-Domínguez, A.; Maier, S.; Pendry, J.; Chilkoti, A.; Smith, D. *Science* 2012, 337, (6098), 1072-1074.
33. Yang, Y.; Zhu, D.; Yan, W.; Agarwal, A.; Zheng, M.; Joannopoulos, J. D.; Lalanne, P.; Christensen, T.; Berggren, K. K.; Soljačić, M. *Nature* 2019, 576, (7786), 248-252.
34. Savage, K. J.; Hawkeye, M. M.; Esteban, R.; Borisov, A. G.; Aizpurua, J.; Baumberg, J. J. *Nature* 2012, 491, (7425), 574.
35. Zhu, W.; Esteban, R.; Borisov, A. G.; Baumberg, J. J.; Nordlander, P.; Lezec, H. J.; Aizpurua, J.; Crozier, K. B. *Nat. Commun.* 2016, 7, 11495.
36. Yang, Y.; Miller, O. D.; Christensen, T.; Joannopoulos, J. D.; Soljacic, M. *Nano Lett.* 2017, 17, (5), 3238-3245.
37. Sugimoto, H.; Fujii, M. *ACS Photonics* 2018, 5, (5), 1986-1993.
38. Kats, M. A.; Blanchard, R.; Genevet, P.; Capasso, F. *Nature materials* 2013, 12, (1), 20-24.
39. Shirahata, N.; Hirakawa, D.; Masuda, Y.; Sakka, Y. *Langmuir* 2013, 29, (24), 7401-7410.
40. Avrutsky, I.; Soref, R.; Buchwald, W. *Opt. Express* 2010, 18, (1), 348-363.
41. Palik, E. D., *Handbook of optical constants of solids*. Academic press: 1998; Vol. 3.
42. Johnson, P. B.; Christy, R.-W. *Phys. Rev. B* 1972, 6, (12), 4370.
43. Aspnes, D. E.; Studna, A. *Phys. Rev. B* 1983, 27, (2), 985.
44. Ciesielski, A.; Skowronski, L.; Pacuski, W.; Szoplik, T. *Mater. Sci. Semicon. Proc.* 2018, 81, 64-67.
45. Tan, S. J.; Zhang, L.; Zhu, D.; Goh, X. M.; Wang, Y. M.; Kumar, K.; Qiu, C.-W.; Yang, J. K. *Nano Lett.* 2014, 14, (7), 4023-4029.
46. Jovanov, V.; Stiebig, H.; Knipp, D. *ACS Photonics* 2017, 5, (2), 378-383.
47. Li, Z.; Butun, S.; Aydin, K. *ACS Photonics* 2015, 2, (2), 183-188.

48. Song, M.; Wang, D.; Peana, S.; Choudhury, S.; Nyga, P.; Kudyshev, Z. A.; Yu, H.; Boltasseva, A.; Shalaev, V. M.; Kildishev, A. V. *Applied Physics Reviews* 2019, 6, (4), 041308.
49. Nunley, T. N.; Fernando, N. S.; Samarasingha, N.; Moya, J. M.; Nelson, C. M.; Medina, A. A.; Zollner, S. *Journal of Vacuum Science & Technology B, Nanotechnology and Microelectronics: Materials, Processing, Measurement, and Phenomena* 2016, 34, (6), 061205.
50. Goh, X. M.; Ng, R. J. H.; Wang, S.; Tan, S. J.; Yang, J. K. *ACS Photonics* 2016, 3, (6), 1000-1009.